Available online at www.sciencedirect.com
ScienceDirect
International Journal of Heat and Mass Transfer 51 (2008) 3127–3143
International Journal of HEAT and MASS TRANSFER
www.elsevier.com/locate/ijhmt

Transient modeling and analysis of a passive liquid-feed DMFC

Bin Xiao, Amir Faghri *

Department of Mechanical Engineering, University of Connecticut, 261 Glenbrook Road, Unit 2337, Storrs, CT 06269, United States

Received 14 July 2007; received in revised form 21 August 2007
Available online 22 October 2007

Abstract

A two-dimensional, transient, multi-phase, multi-component model has been developed for a liquid-feed DMFC delivery system including the fuel cell itself. The model considers the mass transport in the feed delivery system attached to the anode inlet of the fuel cell, and the effect of coupled heat and mass transfer under ambient conditions. The results are compared with the existing experimental data with a high level of agreement. The effects of feed methanol concentration in the reservoir and current density on mass transport and performance of DMFC system are revealed. When initial feed concentration in the reservoir decreases, methanol crossover is minimized, but the duration of cell performance is shortened and fuel cell temperature decreases. The anodic overpotential and its increasing rate become higher, while the decreasing rates of solution leftover and methanol concentration in the reservoir become lower. When current density increases, the duration of the cell performance is shortened. While the anodic overpotential and its increasing rate, cell temperature, decreasing rates of methanol crossover, solution leftover and methanol concentration in the reservoir increase.

1. Introduction

Direct methanol fuel cells are a promising power source for portable applications that have the advantages of high efficiency, reliability, flexibility, durability and easy maintenance. Without external delivery devices such as pumps, fans and blowers, DMFCs can be stored in their liquid or vapor state and delivered by passive means [1–7]. The passive DMFCs utilize porous layers with wicking materials to deliver the dilute methanol solution to the fuel cell, mainly by diffusion, and control the methanol concentration in the anode inlet.

Two predominant issues that hinder the application of direct methanol fuel cell (DMFC) technology are low kinetics of methanol electro-oxidation on the anode catalyst, and crossover of un-reacted methanol from the anode to the cathode. The crossover of methanol lowers the system efficiency, and adversely affects the oxygen cathode due to corrosion through the membrane and oxidation at the cathode [8–11], resulting in poor cell performance. Some work has also been focused on developing a more active methanol electro-oxidation catalyst and mechanism, including experimental studies on the catalyst structures of Pt–Ru and the effects of the anode electrochemical reaction on fuel cell performance [12–16].

Since a DMFC includes complicated phenomena such as electrochemical reactions, hydrodynamics, multi-component transport and heat transfer, it is necessary to develop DMFC models as computer-aid tools for the design and optimization of a fuel cell, and to better understand the interacting electrochemical and transport phenomena. Most of the one-dimensional, single-phase models are based on the isothermal assumption [17–19] except that a few papers took the ambient thermal influence into account [20,21]. Baxer et al. [17] developed a mathematical model for the liquid-feed DMFC, mainly on the anode catalyst layer, which predicted the amount of methanol crossover through the membrane at given current densities and the necessary fuel flow rate to maintain water-soluble levels of carbon dioxide in the anode's liquid-filled pores. Garcia et al. [18] solved a semi-analytical model for a liquid-feed DMFC including the anode

* Corresponding author. Tel.: +1 860 486 0419; fax: +1 860 486 5088.
E-mail address: amir.faghri@uconn.edu (A. Faghri).

0017-9310/$ - see front matter © 2007 Elsevier Ltd. All rights reserved.
doi:10.1016/j.ijheatmasstransfer.2007.08.022

Nomenclature

A	area of fuel cell (m^2)
a	constant in coefficient matrix
a_{ox}	specific area for oxidation (m^{-1})
a_{red}	specific area for reduction (m^{-1})
b	element in solution matrix
$\mathbf{B}$	coefficient matrix for Stefan–Maxwell (s/m^2)
c_{MeOH}	methanol concentration in liquid (mol/cm^3)
c_{H_2O}	water concentration in liquid (mol/cm^3)
d_g	characteristic length of gas phase (m)
D_{ij}	binary diffusivity (m^2/s)
$D_{eff,ij}$	effective diffusivity of gas phase (m^2/s)
F	Faraday constant (coulomb/mol)
h_{fg}	latent heat of vaporization (J/kg)
h_m	mass transfer coefficient (ms)
$I_{0,ref}^{MeOH}$	oxidation exchange current density (A/cm^2)
$I_{0,ref}^{O_2}$	reduction exchange current density (A/cm^2)
$\mathbf{I}$	current density (A/cm^2)
$\mathbf{I}_p$	proton current density ($proton/cm^2\ s$)
$\mathbf{J}$	mass flux ($kg/m^2\ s$)
$J(s)$	Leverette function
k_{rg}	relative permeability of gas phase
k_{rl}	relative permeability of liquid phase
$\mathbf{K}$	permeability (m^{-2})
$\dot{m}'''$	mass source ($kg/m^3\ s$)
M_i	molecular weight of component i (kg/mol)
M_g	molecular weight of gas (kg/mol)
M_l	molecular weight of liquid (kg/mol)
$\mathbf{n}$	surface normal vector
n_d	electro-osmotic drag coeff. (mol/mol)
p_c	capillary pressure (Pa)
p_l	liquid pressure (Pa)
p_g	gas pressure (Pa)
R_u	ideal gas constant ($J/mol \cdot K$)
R_Ω	resistance (Ω)
R_{ox}	oxidation reaction rate (A/m^3)
R_{red}	reduction reaction rate (A/m^3)
Re_ε	pore Reynolds number
t	time (s)
T	temperature (K)
s	liquid saturation
$\mathbf{V}_k$	velocity of phase k (m/s)
$\langle \mathbf{V}_k \rangle^k$	intrinsic phase velocity of phase k (m/s)
V	volume (m^3)
x_{MeOH}	mole fraction of methanol in liquid (mol/mol)
x	distance in x-direction (m)
y	distance in y-direction (m)

Greek symbols

α_l	liquid volume fraction
$\alpha_{l,MeOH}$	volume fraction of MeOH in liquid phase
α_a	anode transfer coefficient
α_c	cathode transfer coefficient
ε	porosity
η	fuel consumption efficiency
η_a	anodic overpotential (V)
η_c	cathodic overpotential (V)
λ	oxidation constant (mol/cm^3)
μ	viscosity ($N\ s/m^2$)
θ	contact angle between liquid and solid (radians)
σ	surface tension (N/m)
σ_c	electrical conductivity of carbon phase ($\Omega^{-1}\ m^{-1}$)
σ_m	proton conductivity of membrane phase ($\Omega^{-1}\ m^{-1}$)
ρ	density (kg/m^3)
τ	tortuosity
$\omega_{g,i}$	mass fraction of gas (kg/kg)
$\omega_{l,i}$	mass fraction of liquid (kg/kg)
ΔV	control volume (m^3)
ΔT	time step (s)

Subscripts

acl	anode catalyst layer
agdl	anode gas diffusion layer
ccl	cathode catalyst layer
cgdl	cathode gas diffusion layer
e	entrance
g	gas
i	component i
ini	initial
j	component j
l	liquid
m	membrane
n	neighboring cells
r	methanol reservoir
R	due to chemical reaction
T	due to mass transport (evaporation/condensation)

Superscripts

k	previous iteration
$k+1$	next iteration

gas diffusion and a catalyst layer, as well as the membrane. The model considered the multi-step methanol oxidation reaction at the anode, and the mixed potential of the oxygen cathode due to methanol crossover. Dohle et al. [19] presented a liquid-feed DMFC model that included catalyst layers, membranes and gas diffusion layers. The model calculated mass transport in the layers as well as the electrochemical concentration-dependent reactions in the catalyst layers. The methanol crossover phenomena and the effects of methanol concentration on cell performance were

analyzed. Chen and Zhao [20] presented a theoretical model that incorporates the effects of coupled heat, mass transfer, and electrochemical kinetics in a passive liquid-feed DMFC under ambient conditions. They analyzed the thermal effects on the cell's performance when using different methanol concentrations. Argyropoulos et al. [21] used a thermal model to estimate the temperature profile and heat flows in a liquid-feed DMFC stack based on the energy conservation equation. The model was used to assess the effect of the operating parameters such as temperature gradient, current density, flow rate, and pressure, on the temperature profile along the stack.

Although one-dimensional models can reveal parts of the fuel cell's physicochemical mechanisms and transport phenomena with a relatively short solution time, it is necessary to develop more comprehensive physical models in order to better understand the fuel cell's performance. Some multi-dimensional models for DMFCs have been issued in the recent years [22–26]. Kulikovsky [22] numerically solved a two-dimensional model of a liquid-feed DMFC based on mass and current conservation. The velocity of the liquid was driven by diffusion and electro-osmotic drag. The results showed the influence of the hydraulic permeability of the diffusion layers on methanol crossover. In another paper, Kulikovsky et al. [23] developed a two-dimensional model of a vapor-feed DMFC using a single phase approach. The results for an embedded type of current collector and a conventional geometry were compared. Wang and Wang [24] presented a two-phase, multi-component model of a liquid-feed DMFC using a mixture model. The effects of methanol concentration on cell performance were examined. Rice and Faghri [25] developed a two-dimensional, transient multi-phase, multi-component model of a passive fuel delivery system including the fuel cell itself for a liquid-feed DMFC. The model captured evaporative effects, formulated evaporation and condensation rates in a manner to capture non-equilibrium effects between the phases. In another paper by Rice and Faghri [26], the above model was further improved by considering thermal effects, continuous and discontinuous limitations as well as the probabilistic spread of the porous properties. They also added physical characteristics qualitatively to portray the departure of carbon dioxide from the anode side of the fuel cell.

Ge and Liu [27] presented a three-dimensional, two-phase, multi-component model for a liquid-fed DMFC. Both liquid and gas phases were considered in the entire anode, including the channel, the diffusion layer and the catalyst layer; while at the cathode, two phases are considered in the gas diffusion layer and the catalyst layer but only single gas phase is considered in the channels. For electrochemical kinetics, the Tafel equation incorporating the effects of two phases was used at both the cathode and anode sides. The fuel and oxidant flow in the gas channels were assumed to be laminar and the gas mixtures are assumed to be perfect gases. All phases were assumed to be continuous. Parameters such as gas volume fraction and liquid saturation were assumed to be volume-averaged properties to accommodate a macroscopic continuum approach in the porous media. Liquid water was assumed to be homogeneously distributed within each control volume. At the walls and the interface with the collector plate shoulder, no-slip velocity boundary conditions were used. Neumann-type boundary conditions were used for velocity at the channel outlets. At the interface between the catalyst layer and membrane, the velocity was assumed to be zero. For all species equations, the Neumann boundary conditions were applied at all the outlets, solid walls and symmetry surfaces.

Liu and Wang [28] developed a three-dimensional, two-phase model for DMFCs, in particular considering water transport and treating the catalyst layer explicitly as a component rather than an interface without thickness. The DMFC model was based on the multi-phase mixture

Table 1
A summary of features of selected DMFC models developed in recent years

Author(s)	Dimension	State[a]	Thermal effect	Phase[b]	Feed solution	Delivery manner	Non-equilibrium[c]	Stefan–Maxwell[d]
Baxter et al. [17]	1-D	SS	No	M-EC	Liquid feed	Active	No	No
Garcia et al. [18]	1-D	SS	No	S	Liquid feed	Active	No	No
Dohle et al. [19]	1-D	SS	No	S	Liquid feed	Active	No	Yes
Chen and Zhao [20]	1-D	SS	Yes	M-EC	Liquid feed	Passive	No	No
Argyropoulos et al. [21]	1-D	SS	Yes	M-M^2	Liquid feed	Active	No	No
Kulikovsky [22]	2-D	SS	No	M-EC	Liquid feed	Active	No	Yes
Kulikovsky et al. [23]	2-D	SS	No	S	Vapor feed	Active	No	Yes
Wang and Wang [24]	2-D	SS	No	M-M^2	Liquid feed	Active	No	Yes
Rice and Faghri [25]	2-D	TR	No	M-MFM	Liquid feed	Passive	Yes	Yes
Rice and Faghri [26]	2-D	TR	Yes	M-MFM	Liquid feed	Passive	No	Yes
Ge and Liu [27]	3-D	SS	No	M-M^2	Liquid feed	Active	No	No
Liu and Wang [28]	3-D	TR	No	M-M^2	Liquid feed	Active	No	No

[a] SS: Steady state; TR: transient.
[b] M: multi-phase; S: single phase; EC: effective coefficient method for each phase; M^2: multiphase mixture model; MFM: multi-fluid model.
[c] Non-equilibrium: non-equilibrium in the phases.
[d] Stefan–Maxwell: a diffusion model for gas species transport.

formulation and encompasses all components in a DMFC using a single computational domain. The specific assumptions made in this model include: (i) incompressible gas mixture, (ii) laminar flow, (iii) isothermal cells, (iv)isotropic and homogeneous porous GDL, characterized by an effective porosity and permeability, and (v) negligible potential drop due to ohmic resistance in the electronically conductive solid matrix of GDL and catalyst layers, as well as bipolar plates. Furthermore, a homogeneous flow was assumed for the two-phase flow through channels of both anode and cathode.

A summary of major features of the above DMFC models is listed in Table 1. More literature regarding the fundamental models and key issues in fuel cells were reviewed by Refs. [29,30]. In an innovative passive DMFC delivery system developed by Faghri and Guo [3], a reservoir is attached to the anode side of the fuel cell, which is filled with a predetermined concentration of methanol solution. The methanol feed concentration in the reservoir decreases as the methanol solution flows downward, which is assumed to be constant by other models, for simplicity. By taking into consideration the variation of the feed concentration at the reservoir in the operation of the passive DMFC system, a comprehensive, transient, two-dimensional model that includes multi-component and multiphase transport through the whole system was developed in this work. The model also considered the convective heat and mass transfer effects and non-equilibrium in phases in the present study.

2. Mathematical model

The schematic of a passive liquid-feed DMFC delivery system and the membrane exchange assembly is illustrated in Fig. 1. The system can be divided into four parts: methanol delivery, which includes a reservoir filled with a predetermined dilute methanol solution and also includes the layer made of hydrophilic materials that deliver the methanol to the fuel cell and control the methanol concentration at the anode side; a fuel cell, which includes anode and cathode diffusion layers, catalyst layers and a polymer electrolyte membrane; an air-breathing part made of hydrophobic materials to prevent water droplets from forming on the cathode side; and current collectors connected to external circuits to produce power.

The passive liquid-feed DMFC system in this study is a multi-phase problem in porous media: methanol and water are the only components considered in the liquid phase, while methanol, water, oxygen, carbon dioxide and nitrogen exist in the gas phase. The volume averaging for liquid and gaseous velocities for each individual phase within a control volume are applied to accommodate the fluid flow in current DMFC model:

$$\langle \mathbf{V}_l \rangle^l = \frac{1}{V_l}\int_{V_l} \mathbf{V}_l \, dV, \quad \langle \mathbf{V}_g \rangle^g = \frac{1}{V_l}\int_{V_g} \mathbf{V}_g \, dV \tag{1}$$

The simulation is based on the solutions of the governing equations in the liquid and gas phases, including continuity equations, momentum equations, species equations, energy equations and electrochemical equations (potential equations), which are described as follows.

2.1. Continuity equations

Assuming local thermodynamic equilibrium prevails at the phase interface, the generic continuity equations for the liquid and gas phases in the DMFC system, in terms of liquid saturation, s, and the volume-averaged velocities, are described by the multi-fluid model [32]:

$$\frac{\partial}{\partial t}(\varepsilon s \rho_l) + \nabla \cdot (\varepsilon s \rho_l \langle \mathbf{V}_l \rangle^l) = \dot{m}_l''' \tag{2}$$

$$\frac{\partial}{\partial t}(\varepsilon (1-s) \rho_g) + \nabla \cdot (\varepsilon (1-s) \rho_g \langle \mathbf{V}_g \rangle^g) = \dot{m}_g''' \tag{3}$$

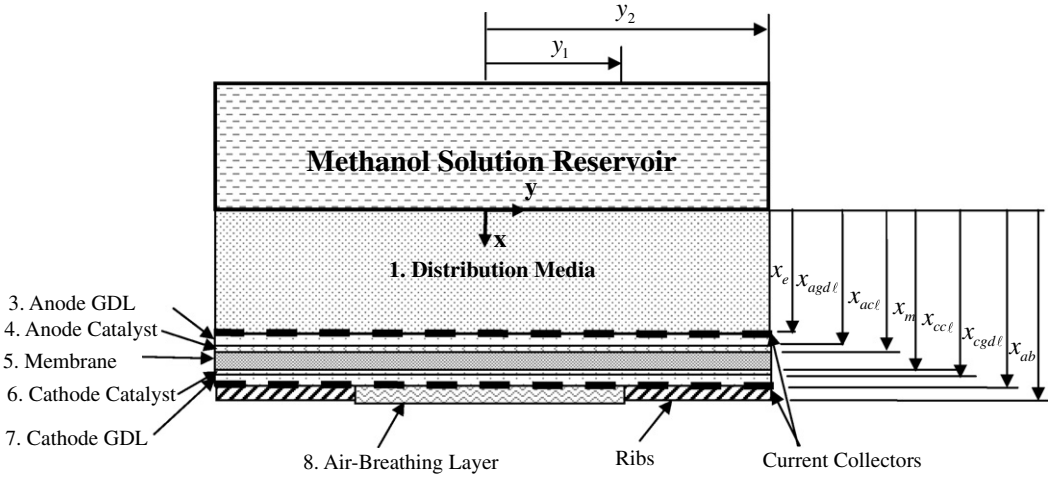

Fig. 1. Schematic diagram of a passive liquid-feed DMFC.

where the mass generation terms are a sum of the reaction rates (subscript R) due to chemical reactions at catalysts and the mass transfer rates from the gas to the liquid phase (subscript T) of each component.

$$\dot{m}'''_{\mathrm{l}} = \sum_i \dot{m}'''_{\mathrm{R,\,l},i} + \sum_i \dot{m}'''_{\mathrm{T,\,gl},i} \tag{4}$$

$$\dot{m}'''_{\mathrm{g}} = \sum_i \dot{m}'''_{\mathrm{R,\,g},i} - \sum_i \dot{m}'''_{\mathrm{T,\,gl},i} \tag{5}$$

2.2. Momentum equations

Since the liquid/gas velocities are very small and the Reynolds number is much less than unity, the inertial terms in the momentum equations can be neglected without compromising the accuracy of the velocity solution. Therefore, by considering the electro-osmotic drag term caused by ion movement in water under the electric field (electro-osmotic effect), the liquid and gaseous momentum equations in porous media can be described by Darcy's law as follows:

$$\varepsilon s\langle \mathbf{V}_{\mathrm{l}}\rangle^{l} = -\frac{k_{\mathrm{rl}}\mathbf{K}}{\mu_{\mathrm{l}}}(\nabla p_{\mathrm{l}} - \rho_{\mathrm{l}}\mathbf{g}) + \frac{n_d M_{\mathrm{l}}}{\rho_{\mathrm{l}}}\frac{\mathbf{I}_p}{F} \tag{6}$$

$$\varepsilon(1-s)\langle \mathbf{V}_{\mathrm{g}}\rangle^{g} = -\frac{k_{\mathrm{rg}}\mathbf{K}}{\mu_{\mathrm{g}}}(\nabla p_{\mathrm{g}} - \rho_{\mathrm{g}}\mathbf{g}) \tag{7}$$

The first term on the right side of Eqs. (6) and (7) represents the driven force of the fluid velocity caused by pressure gradient and gravity. The second term in Eq. (6) is the electro-osmotic drag [31] force through the membrane of the DMFC. The increase in viscous resistance due to each void being partially filled with a particular phase is defined as relative permeability [33].

$$k_{\mathrm{rl}} = s^3 \tag{8}$$

$$k_{\mathrm{rg}} = (1-s)^3 \tag{9}$$

The capillary pressure depends on the interfacial tension between liquid and vapor phases in the porous media, which can be described by the cubic Leverette function:

$$p_{\mathrm{c}} = p_{\mathrm{g}} - p_{\mathrm{l}} = \sigma\cos\theta\left(\frac{\varepsilon}{K}\right)^{1/2} J(s) \tag{10}$$

$$J(s) = \begin{cases} 1.417(1-s) - 2.120(1-s)^2 + 1.263(1-s)^3 \\ \quad \theta < \pi/2.0 \\ 1.417s - 2.120s^2 + 1.263s^3 \\ \quad \theta \geqslant \pi/2.0 \end{cases} \tag{11}$$

2.3. Species equations

Assuming incompressible gas components and laminar flow due to the low Reynolds number, the species equations in liquid and gas using the multi-fluid model [32] are:

$$\frac{\partial}{\partial t}(\varepsilon s\rho_{\mathrm{l}}\omega_{\mathrm{l},i}) + \nabla\cdot(\dot{\mathbf{m}}''_{\mathrm{l},i}) = \dot{m}'''_{\mathrm{l},i} \tag{12}$$

$$\frac{\partial}{\partial t}(\varepsilon(1-s)\rho_{\mathrm{g}}\omega_{\mathrm{g},i}) + \nabla\cdot(\dot{\mathbf{m}}''_{\mathrm{g},i}) = \dot{m}'''_{\mathrm{g},i} \tag{13}$$

The total mass flux (the sum of the advection and diffusion fluxes) of each species is represented by $\dot{\mathbf{m}}_{\mathrm{l},i}$ and $\dot{\mathbf{m}}_{\mathrm{g},i}$, in the liquid and gas phase, respectively.

$$\dot{\mathbf{m}}''_{\mathrm{l},i} = \varepsilon s\rho_{\mathrm{l}}\langle \mathbf{V}_{\mathrm{l}}\rangle^{l}\omega_{\mathrm{l},i} - [\varepsilon s]^{\tau}\rho_{\mathrm{l}}D_{\mathrm{l},12}\nabla\omega_{\mathrm{l},i} \tag{14}$$

$$\dot{\mathbf{m}}''_{\mathrm{g},i} = \varepsilon(1-s)\rho_{\mathrm{g}}\langle \mathbf{V}_{\mathrm{g}}\rangle^{g}\omega_{\mathrm{g},i} - \sum_{j=1}^{N-1}[\varepsilon(1-s)]^{\tau}\rho_{\mathrm{g}}D_{\mathrm{eff},ij}\nabla\omega_{\mathrm{g},j} \tag{15}$$

The effective diffusivity in the gas phase can be calculated from the Stefan–Maxwell equation after some mathematical manipulation.

$$[D_{\mathrm{eff},ij}] = \mathbf{A}^{-1}\mathbf{B} \tag{16}$$

$$A_{ii} = -\frac{\omega_{\mathrm{g},i}M_{\mathrm{g}}^2}{D_{iN}M_N M_i} - \sum_{\substack{k=1\\k\neq i}}^{N}\frac{\omega_{\mathrm{g},k}M_{\mathrm{g}}^2}{D_{ik}M_k M_i};$$

$$A_{ij} = \omega_{\mathrm{g},i}\frac{M_{\mathrm{g}}^2}{M_i}\left(\frac{1}{D_{ij}M_j} - \frac{1}{D_{iN}M_N}\right),\quad i\neq j \tag{17}$$

$$B_{ii} = -\frac{M_{\mathrm{g}}}{M_i}\left(1 - \frac{M_{\mathrm{g}}\omega_{\mathrm{g},i}}{M_i}\right) - \frac{M_{\mathrm{g}}^2\omega_{\mathrm{g},i}}{M_i M_N};$$

$$B_{ij} = \frac{M_{\mathrm{g}}^2\omega_{\mathrm{g},i}}{M_i}\left(\frac{1}{M_j} - \frac{1}{M_N}\right),\quad i\neq j \tag{18}$$

Table 2
Boundary conditions for the passive DMFC model

Governing equations	$x=0$	$x=x_{\mathrm{agdl}}$	$x=x_{\mathrm{acl}}$	$x=x_m$	$x=x_{\mathrm{ccl}}$	$x=x_{\mathrm{cgdl}}$	$x=x_{ab}$
Momentum	$\nabla p_{\mathrm{g}}\cdot\mathbf{n}=0$ $p_{\mathrm{l}}=0$	N/A N/A	N/A N/A	N/A N/A	N/A N/A	N/A N/A	$p_{\mathrm{g}}=0$ $\nabla p_{\mathrm{l}}\cdot\mathbf{n}=0$
Gas transport	$\nabla\omega_{g,i}=0$	N/A	N/A	N/A	N/A	N/A	$-[\varepsilon(1-s)]^{\tau}\nabla\omega_{\mathrm{g},i}\cdot\mathbf{n}$ $=h_m(\omega_{\mathrm{g},i}-\omega_{\mathrm{g},i,\infty})$
Liquid transport	$\dot{\mathbf{m}}''=\varepsilon s\rho_{\mathrm{l}}\langle\mathbf{V}_{\mathrm{l}}\rangle^{\mathrm{l}}\omega_{\mathrm{l,MeOH}}$ $+h_m(\omega_{\mathrm{res,MeOH}}-\omega_{\mathrm{l,MeOH}})$	N/A	N/A	N/A	N/A	N/A	$\nabla\omega_{\mathrm{l},i}\cdot\ \mathbf{n}=0$
Membrane potentials	N/A	$\nabla\phi_m\cdot\mathbf{n}=0$	N/A	N/A	$\nabla\phi_m\cdot\mathbf{n}=0$	N/A	N/A
Catalyst potential	$-\sigma_{\mathrm{c}}\frac{\partial\phi_{\mathrm{c}}}{\partial x}=I_{\mathrm{cell}}$	N/A	$\nabla\phi_{\mathrm{c}}\cdot\mathbf{n}=0$	$\nabla\phi_{\mathrm{c}}\cdot\mathbf{n}=0$	N/A	$\phi_{\mathrm{c}}=V_{\mathrm{cell}}$	N/A
Energy	$T=T_\infty$	N/A	N/A	N/A	N/A	N/A	$-k_{\mathrm{eff}}\nabla T\cdot\mathbf{n}$ $=h(T-T_{\mathrm{eff}})$

For the condensable gases, the liquid and vapor phases are considered to be in thermal dynamic equilibrium. Equilibrium is found using Raoult's law, where the saturation pressure is calculated by the Clausius–Clapeyron equation.

Table 3
Physicochemical properties [37]

Parameter		Value	
	$K/\varepsilon/\tau$	θ (H_2O/MeOH)	p_{shift}
	(m^2/unitless/unitless)	(radians) (Pa)	
Pref. wick.	2.5e−13/ 0.8/ 1	$\pi/0$	$(\theta < \pi/2)$ −100, $(\theta > \pi/2)$ 50
Non. pref.	1e−10/ 0.8/ 1	0/0	−200
agdl	1e−11/ 0.7/ 1	0/0	−200
acl	2.5e−12/ 0.6/ 1.8	0/0	−200
mem.	1e−13/ 0.5/ 1.8	0/0	0
ccl	2.5e−11/ 0.6/ 1.8	$\frac{\pi}{3}/0$	−200
cgdl	1e−10/ 0.7/ 1	π/π	50
Diffusivity, gas phase, $D_{ij} = D_{ji}$ (m^2/s)	O_2/CO_2	0.159×10^{-4}	
	O_2/H_2O	0.244×10^{-4}	
	$O2/N_2$	0.202×10^{-4}	At 293 K
	CO_2/H_2O	0.162×10^{-4}	1 bar
	CO_2/N_2	0.160×10^{-4}	
	H_2O/N_2	0.242×10^{-4}	
	O_2/MeOH, CO_2/MeOH, H_2O/MeOH, MeOH/N_2	$\begin{pmatrix} -0.06954+ \\ 4.5986 \times 10^{-4}T+ \\ 9.4979 \times 10^{-7}T^2 \end{pmatrix} \times 10^{-4}$	
Diffusivity, liquid phase (m^2/s)	MeOH/H_2O	$10^{(-5.4163-999.778/T)}$	
Viscosity, μ (Ns/m^2)	Gas phase	$0.1846 \cdot 10^{-4}$	
	H_2O	8.55×1010^{-4}	
	MeOH	5.390×1010^{-4}	
Density, $\rho_{l,i}$ (kg/m^3)	H_2O	$\exp\begin{pmatrix} 6.9094 - 2.0146 \times 10^{-5}(T-273)- \\ 5.9868 \times 10^{-6}(T-273)^2 + 2.5921 \times 10^{-8}(T-273)^3- \\ 9.3244 \times 10^{-11}(T-273)^4 + 1.2103 \times 10^{-13}(T-273)^5 \end{pmatrix}$	
	MeOH	$244.4 \cdot 0.224^{\left(-\left(1-\frac{T}{513}\right)^{\frac{2}{7}}\right)}$	
Electro-osmotic drag coefficient (mol/mol)	n_d	2.5	
Electric conductivity, (Ω^{-1} m^{-1})	σ_c	4000	
	σ_m	3.4	
Transfer coefficient	α_a	0.52	
	α_c	1.55	
Specific area (m^{-1})	a_{ox}	16.09	
	a_{red}	$\frac{1}{x_{ccl}-x_m} = 43478$	
Exchange current	$I_{0,ref}^{MeOH}$	$94.25\exp(35570/R(1/353 - 1/T))$	
Density (A/m^2)	$I_{0,ref}^{O_2}$	$0.04222\ \exp(732000/R(1/353 - 1/T))$	
Oxidation constant (mol/cm^3)	λ	2.4×10^{-9}	
Reduction reference mass fraction (kg/kg)	$m_{O_2,ref}$	0.23	
Thermodynamic potential (V)	U^{MeOH}	−0.0229	
	U^{O_2}	1.24	
Distance (m)	x_e	3.2×10^{-4}	
	$x_{agdl} - x_e$	1.5×10^{-4}	
	$x_{acl} - x_{agdl}$	2.3×10^{-5}	
	$x_m - x_{acl}$	1.8×10^{-4}	
	$x_{ccl} - x_m$	2.3×10^{-5}	
	$x_{cgdl} - x_{ccl}$	1.5×10^{-4}	
	$x_{ab} - x_{cgdl}$	1.5×10^{-4}	
	y_2	5×10^{-3}	
	y_1	3.25×10^{-3}	

$$\omega_{g,i} = \beta_i \omega_{l,i}$$
$$\beta_i = \frac{M_l p_{ref}}{M_g p_{op}} \exp\left(\frac{h_{fg} M_i}{R}\left(\frac{1}{T_{ref}} - \frac{1}{T}\right)\right) \quad (19)$$

2.4. Energy equations

To describe the distribution of temperature in the DMFC system, the following assumptions are made to simplify the mathematical treatment: (i) the specific heat is assumed to be constant; (ii) heat transfer takes place through the bulk fluid flow; (iii) a fully hydrated continuum with effective ionic and electronic conductivities in the membrane. The energy equation can be written as:

$$\frac{\partial}{\partial t}(\varepsilon s \rho_l h_l + \varepsilon(1-s)\rho_g h_g + (1-\varepsilon)h_s) + \sum_i \nabla \cdot (\dot{\mathbf{m}}''_{l,i} h_{l,i} + \dot{\mathbf{m}}''_{g,i} h_{g,i}) = \nabla \cdot (k_{eff} \nabla T) + \nabla \cdot (\phi_m \sigma_m \nabla \phi_m) + \nabla \cdot (\phi_c \sigma_c \nabla \phi_c) \quad (20)$$

The enthalpy can be written as sensible heat, $\bar{h}$, plus the heat of formation, h^0. Taking the species mass balance into consideration, the energy equation can be rewritten in terms of the sensible heat transport and the heat generation terms that coincide with the reaction rates and phase change.

$$\frac{\partial}{\partial t}(\varepsilon s \rho_l \bar{h}_l + \varepsilon(1-s)\rho_g \bar{h}_g + (1-\varepsilon)\bar{h}_s) + \sum_i \nabla \cdot (\dot{\mathbf{m}}''_{l,i} \bar{h}_{l,i} + \dot{\mathbf{m}}''_{g,i} \bar{h}_{g,i}) = \nabla \cdot (k_{eff} \nabla T) - \sum_i \dot{m}'''_{l,i} h^0_{l,i} - \sum_i \dot{m}'''_{g,i} h^0_{g,i} + \nabla \cdot (\phi_m \sigma_m \nabla \phi_m) + \nabla \cdot (\phi_c \sigma_c \nabla \phi_c) \quad (21)$$

The total sensible enthalpy in each phase is based on mass weighted averaging:

$$\bar{h}_l = \sum_i \omega_{l,i} \bar{h}_{l,i} \quad (22)$$

$$\bar{h}_g = \sum_i \omega_{g,i} \bar{h}_{g,i} \quad (23)$$

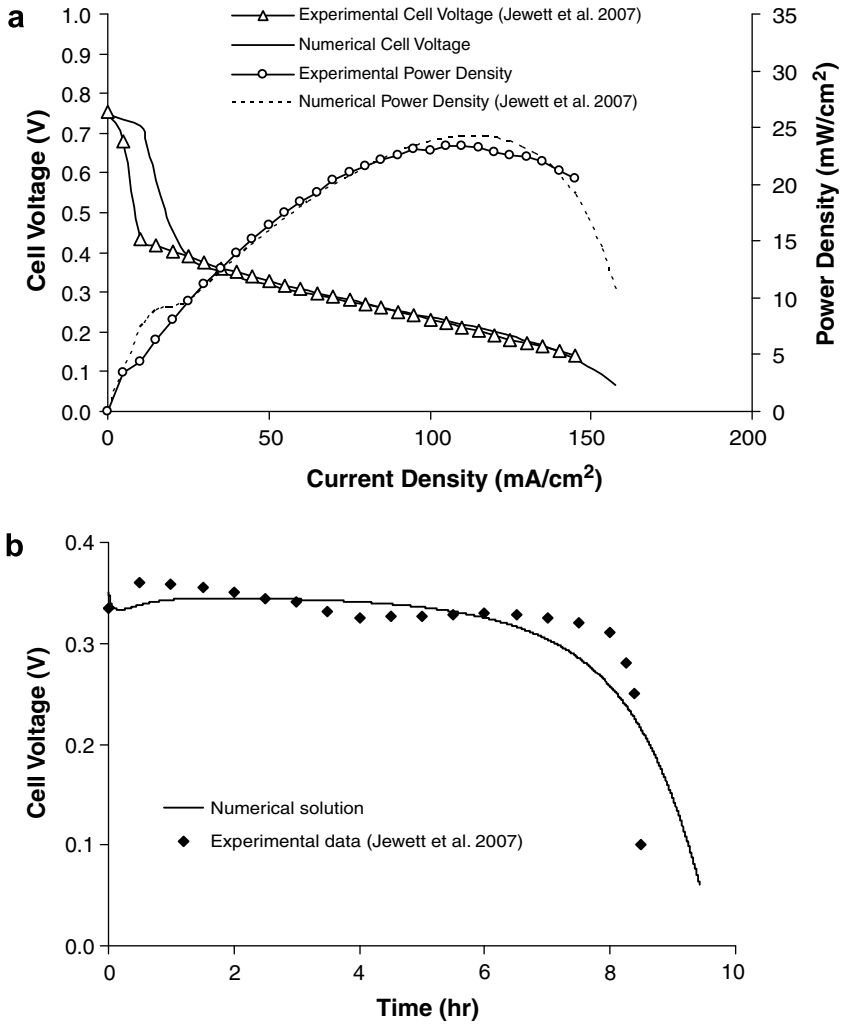

Fig. 2. Verification of numerical results with the initial operation condition of 3 M methanol feed concentration in the reservoir solution. (a) Polarization curves and (b) transient cell voltage with a constant current density of 40 mA/cm^2.

The effective thermal conductivity is:

$$k_{\text{eff}} = \varepsilon s k_{\text{l}} + \varepsilon(1-s)k_{\text{g}} + (1-\varepsilon)k_{\text{s}} \tag{24}$$

2.5. Potential equations

The electrochemistry is modeled to determine the electric potential of the carbon phase and the membrane phases which obey the following governing equations:

$$\nabla \cdot (\sigma_{\text{c}} \nabla \phi_{\text{c}}) - R_{\text{ox}} + R_{\text{red}} = 0 \tag{25}$$

$$\nabla \cdot (\sigma_{\text{m}} \nabla \phi_{\text{m}}) + R_{\text{ox}} - R_{\text{red}} = 0 \tag{26}$$

These equations follow the continuity equation $\nabla j = R$ and Ohm's law $j = \pm \sigma \nabla \varphi$, which implicitly assumes local electroneutrality, i.e., the absence of space charge effects in the membrane and carbon phases. The oxidation and reduction reaction rates are R_{ox} and R_{red}, respectively. Fundamental studies of reaction kinetics may have many complex forms [34] due to the multistage character of reaction, possible parallel pathways with intermediate products and various crystal structure and defects on clusters of catalyst particles related to different fabrication procedure. In terms of the Butler–Volmer theory, the reaction rates in current study are modeled by the Tafel kinetic expression developed by Meyers and Newman [35].

$$R_{\text{ox}} = a_{\text{ox}} I_{0,\text{ref}}^{\text{MeOH}} \frac{c_{\text{MeOH}}}{c_{\text{MeOH}} + \lambda \exp\left(\alpha_{\text{a}} \eta_{\text{a}} \frac{F}{R_u T}\right)} \exp\left(\alpha_{\text{a}} \eta_{\text{a}} \frac{F}{R_u T}\right) \tag{27}$$

$$R_{\text{red}} = a_{\text{red}} I_{0,\text{ref}}^{\text{O}_2} \frac{\omega_{\text{O}_2}}{\omega_{\text{O}_2,ref}} \exp\left(\alpha_{\text{c}} \eta_{\text{c}} \frac{F}{R_u T}\right) \tag{28}$$

The overpotentials at the anode and the cathode are defined by

$$\eta_{\text{a}} = \phi_{\text{c}} - \phi_{\text{m}} - U^{\text{MeOH}} \tag{29}$$

$$\eta_{\text{c}} = U^{\text{O}_2} + \phi_{\text{m}} - \phi_{\text{c}} \tag{30}$$

Assuming the ohmic loss in the electrolyte membrane is negligible, once the value of the overpotentials at the anode and the cathode are calculated, the cell voltage can be determined as follows:

$$V_{\text{cell}} = U^{\text{O}_2} - U^{\text{MeOH}} - \eta_{\text{a}} - \eta_{\text{c}} \tag{31}$$

The reaction rates for the species equations are:

$$\dot{m}'''_{\text{R, l, MeOH}} = -\frac{R_{\text{ox}}}{6F} M_{\text{MeOH}};$$

$$\dot{m}'''_{\text{R, l, H}_2\text{O}} = \left(-\frac{R_{\text{ox}}}{6F} + \frac{R_{\text{red}}}{2F}\right) M_{\text{H}_2\text{O}} \tag{32}$$

$$\dot{m}'''_{\text{R, g, CO}_2} = \frac{R_{\text{ox}}}{6F} M_{\text{CO}_2}, \quad \dot{m}'''_{\text{R, g, O}_2} = -\frac{R_{\text{red}}}{4F} M_{\text{O}_2} \tag{33}$$

2.6. Boundary and Initial conditions

Table 2 contains the boundary conditions used in the passive liquid-feed DMFC model. The boundary conditions in the other parts of the fuel cell system are symmetrical, thus the gradients of the variables are taken to be zero. The heat and mass transfer coefficient is taken from the natural convection correlations on a horizontal surface facing up.

$$h = Nu \frac{k}{L}; \quad Nu = 0.54(GrPr)^{.025};$$

$$Gr = \frac{g\rho|\Delta\rho|L^3}{\mu^2}; \quad h_m = Sh \frac{\rho D_{ij}}{L}; \quad Sh = 0.54(GrSc)^{.025} \tag{34}$$

The heat and mass transfer coefficients at the surface of the air-breathing layer are taken as a horizontal surface facing down.

$$h = Nu \frac{k}{L}; \quad Nu = 0.27(GrPr)^{.025}$$

$$h_m = Sh \frac{\rho D_{ij}}{L}; \quad Sh = 0.27(GrSc)^{.025} \tag{35}$$

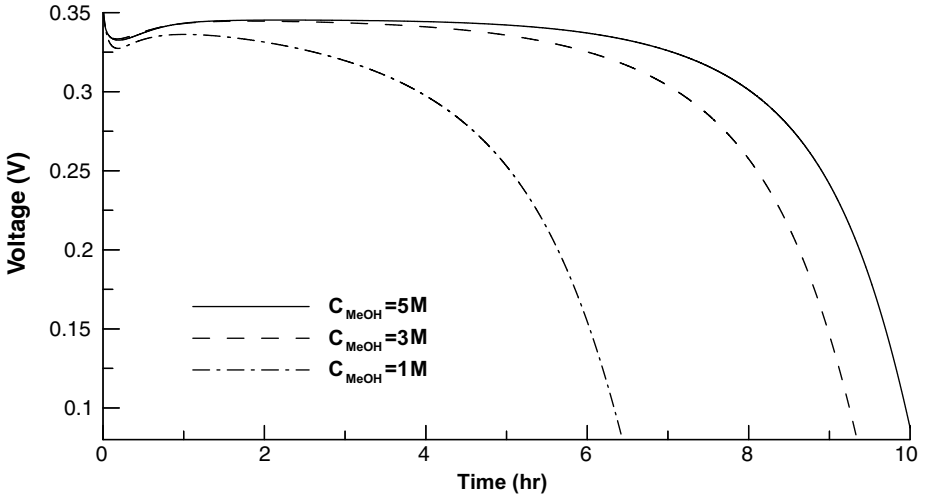

Fig. 3. Variation of cell voltage variations with different initial feed methanol concentrations in the reservoir and a constant current density of 40 mA/cm^2.

The phase saturation is initialized to a value in the layers, depending on the contact angle.

$$\begin{aligned} s &= s_0 \quad \theta < \pi/2 \\ s &= 0 \quad \theta \geqslant \pi/2 \end{aligned} \tag{36}$$

The initial saturation, s_0, was assumed to be unity in the methanol distribution layer and 0.98 in other layers. The methanol distribution layer is initially filled with a feed methanol solution, while every other region contains only water.

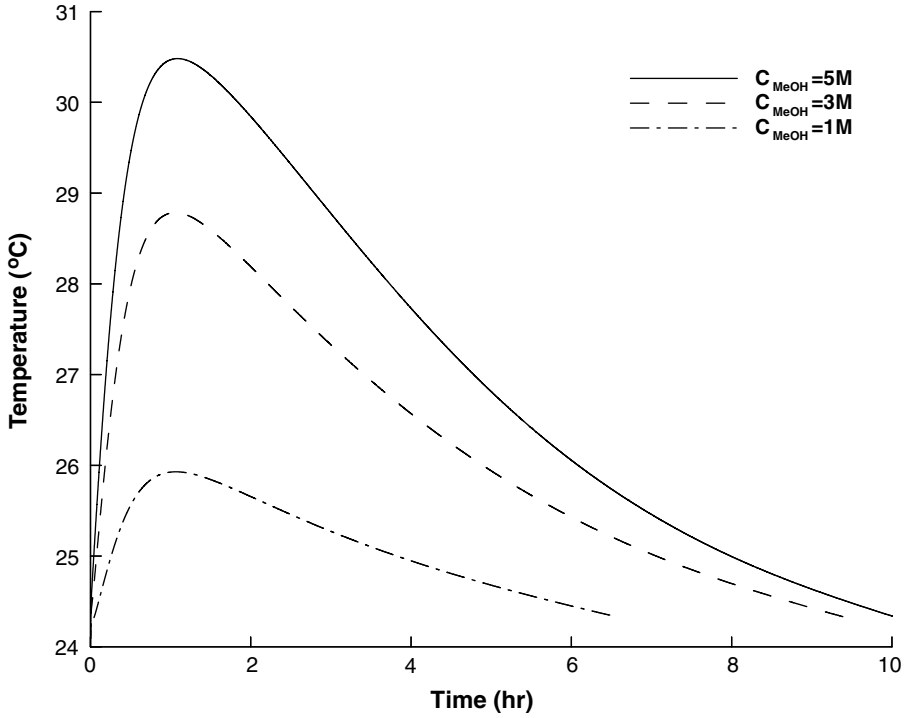

Fig. 4. Variation of temperature rise at the anode inlet with different initial feed methanol concentrations in the reservoir and a constant current density of 40 mA/cm^2.

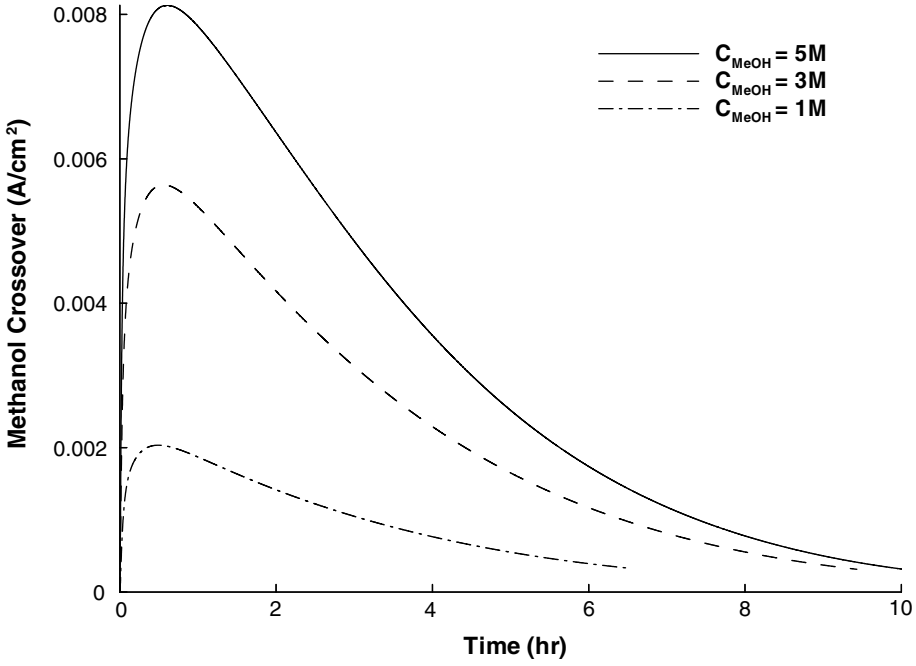

Fig. 5. Variation of total methanol crossover through membrane with different initial feed methanol concentrations in the reservoir and a constant current density of 40 mA/cm^2.

$$\omega_{l,MeOH} = \omega_{1,feed} \quad x < x_e$$
$$\omega_{l,MeOH} = 0 \quad \text{elsewhere} \tag{37}$$

The initial mass fractions of water and methanol vapor are the saturated values if liquid is present, or equivalent to the ambient values if no liquid is present.

$$\omega_{g,i} = \omega_{g,i,sat} \tag{38}$$

The gas mass fractions for the rest of the components are as follows:

$$\omega_{g,CO_2} = 1 - \omega_{g,MeOH} - \omega_{g,H_2O}, \quad \omega_{g,O_2} = \omega_{g,N_2} = 0 \tag{39}$$

'The initial temperature is the assumed ambient temperature.

2.7. Solution procedure

The governing equations for momentum, species, energy and potentials are discretized and solved in a coupled manner by the finite volume method. The flow variables are solved by a Gauss–Siedel iteration scheme. The whole solution procedure for the governing equations is as follows:

1. Assume the cell voltage, solve electric potentials, and update reaction kinetics.
2. Solve for saturation and liquid/gas pressure.
3. Solve species equations and energy equation.
4. Calculate the methanol concentration at reservoir and the cell voltage, treat them as the new guessed ones and update the properties.

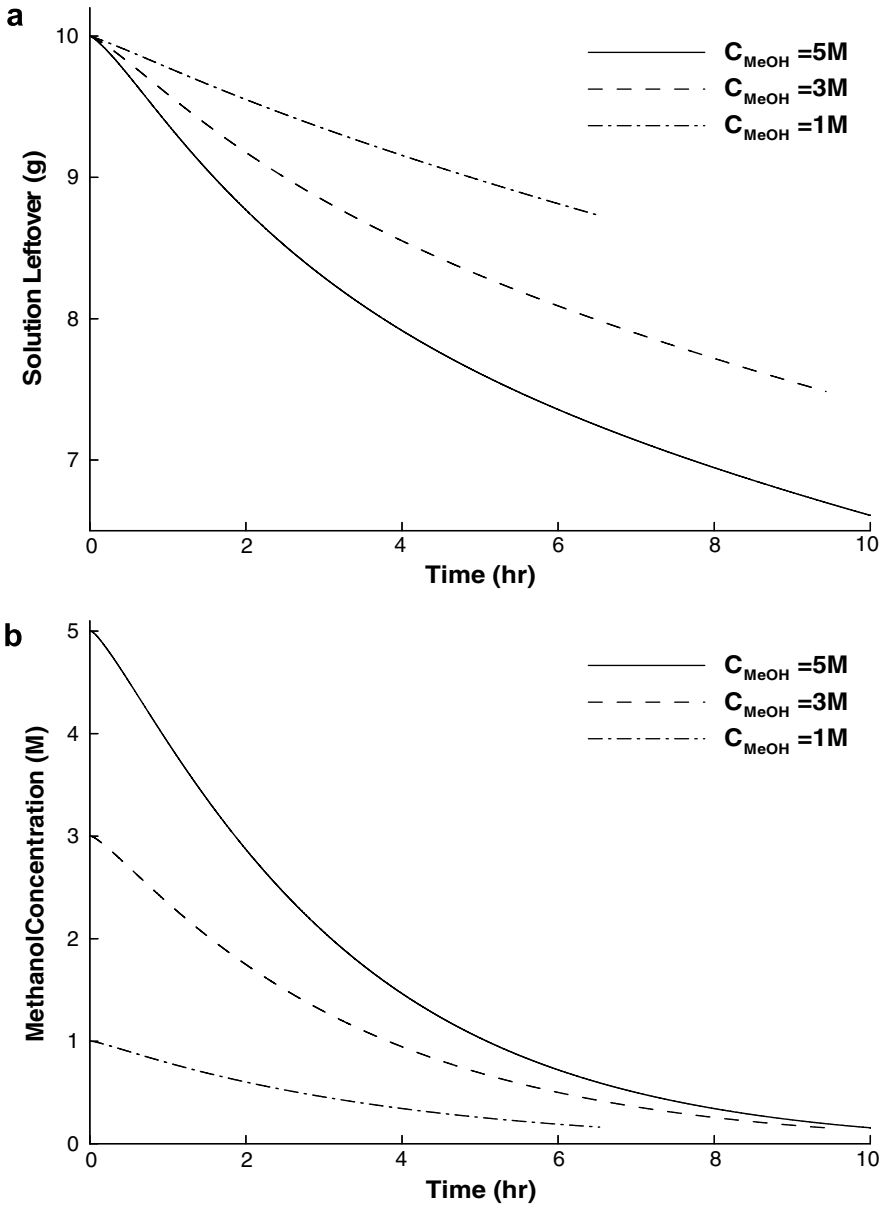

Fig. 6. Variations of (a) solution leftover; (b) methanol concentration the reservoir with different initial feed methanol concentrations in the reservoir and a constant current density of 40 mA/cm^2.

5. Go back to step 1 and repeat until converged, then go to next time step.

In order to get the solutions for the saturation and the liquid/gas pressure, the discretized continuity equations can be written in a general formulation:

$$\begin{aligned} a_{\mathrm{ls}}s + a_{\mathrm{pl}}p_{\mathrm{l}} &= b_{\mathrm{l}} \\ a_{\mathrm{gs}}s + a_{\mathrm{pg}}p_{\mathrm{g}} &= b_{\mathrm{g}} \end{aligned} \tag{40}$$

The liquid and gas pressures are determined by the capillary pressure and can be replaced by the saturation weighted average pressure, $\bar{p}$. Thus, the above equation can be rewritten as follows:

$$\left(a_{\mathrm{ls}} - a_{\mathrm{pl}}\frac{\partial((1-s)p_{\mathrm{c}})^k}{\partial s}\right)s^{k+1} + a_{\mathrm{pl}}\bar{p} = b_{\mathrm{l}} - a_{\mathrm{pl}}\left(-(1-s)p_{\mathrm{c}} + \frac{\partial((1-s)p_{\mathrm{c}})}{\partial s}s\right)^k \tag{41}$$

$$\left(a_{\mathrm{gs}} + a_{\mathrm{pg}}\frac{\partial(sp_{\mathrm{c}})^k}{\partial s}\right)s^{k+1} + a_{\mathrm{pg}}\bar{p} = b_{\mathrm{g}} - a_{\mathrm{pg}}\left(sp_{\mathrm{c}} - \frac{\partial(sp_{\mathrm{c}})}{\partial s}s\right)^k \tag{42}$$

The mass consumption rates in the reservoir are the sums of the reaction and evaporation/condensation rates of the methanol and water in the DMFC, thus the methanol fraction in the reservoir can be calculated by

$$\omega_{\mathrm{r,\ MeOH}} = \frac{\omega_{\mathrm{ini,MeOH}}m_{\mathrm{r,\ ini}} - \left(\sum_i \dot{m}'''_{\mathrm{R,\ l,\ MeOH}} + \sum_i \dot{m}'''_{\mathrm{T,l,g,MeOH}}\right)\Delta V\Delta T}{m_{\mathrm{r,\ ini}} - \left(\sum_i \dot{m}'''_{\mathrm{R,\ l,MeOH}} + \sum_i \dot{m}'''_{\mathrm{T,l,g,MeOH}} + \sum_i \dot{m}'''_{\mathrm{R,\ l,\ H_2O}} + \sum_i \dot{m}'''_{\mathrm{T,l,g,H_2O}}\right)\Delta V\Delta T} \tag{43}$$

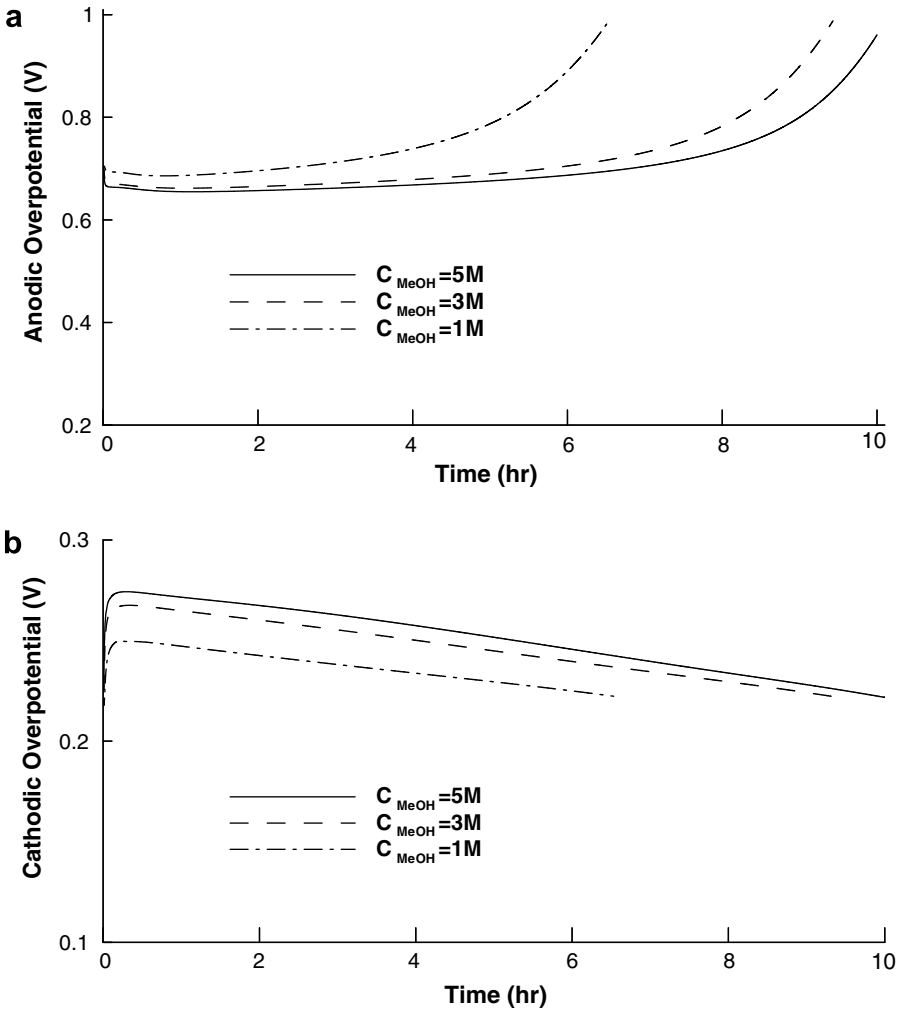

Fig. 7. Variations of (a) anodic overpotential; (b) cathodic overpotential with different initial feed methanol concentrations in the reservoir and a constant current density of 40 mA/cm^2.

The methanol transport from the reservoir to the distribution layer can be represented by

$$\dot{m}'' = \varepsilon s \rho_l \langle \mathbf{V}_l \rangle^l \omega_{l,\mathrm{MeOH}} + h_m(\omega_{r,\mathrm{MeOH}} - \omega_{l,\mathrm{MeOH}}) \tag{44}$$

where $\omega_{1,\mathrm{MeOH}}$ is the methanol concentration at the surface of the distribution layer, $\omega_{r,\mathrm{MeOH}}$ is the feed concentration in the reservoir, and h_m is the mass transfer coefficient proposed by Scott [36] as the following empirical equation:

$$h_m = 1.87 \times 10^{-4} \left(\frac{I_{\mathrm{cell}}}{0.003} \right)^{0.32} \tag{45}$$

The physicochemical properties used in the simulation are listed in Table 3 [25]. The calculation domain for the

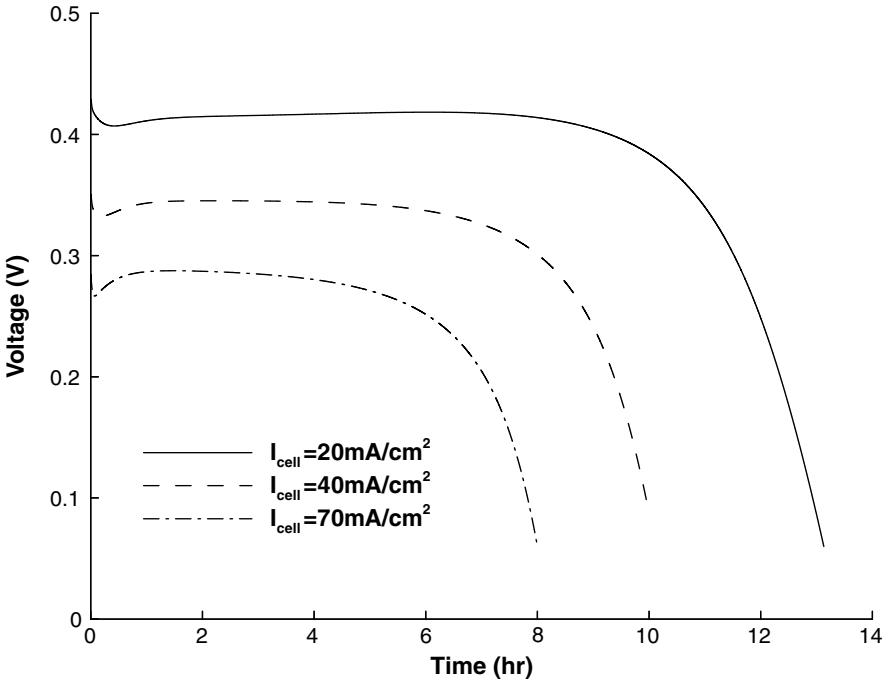

Fig. 8. Variation of cell voltage with different current densities and an initial feed methanol concentration of 5 M in the reservoir.

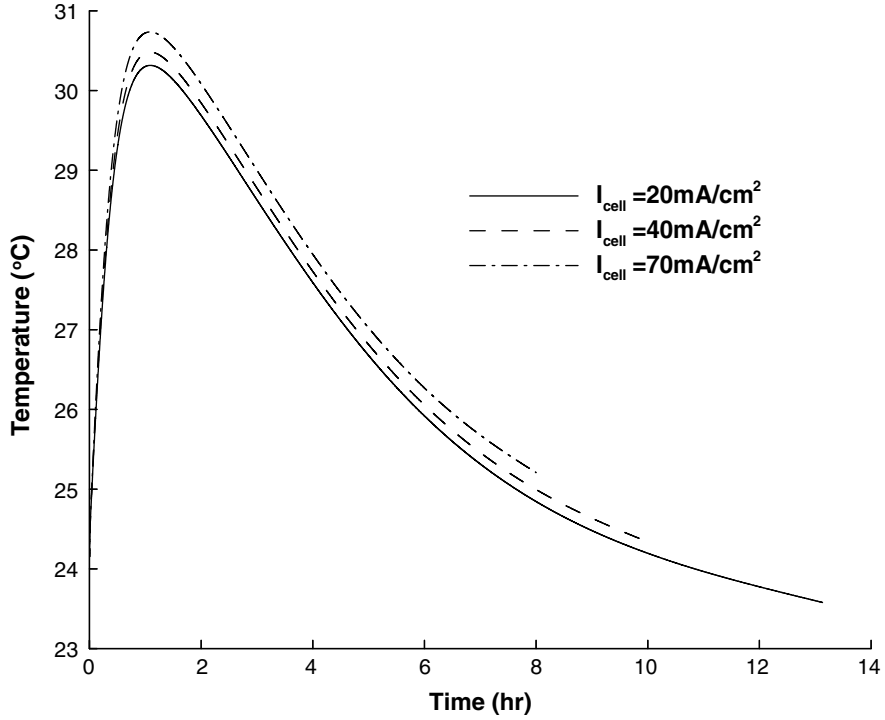

Fig. 9. Variation of temperature at the anode inlet with different current densities and an initial feed methanol concentration of 5 M in the reservoir.

DMFC simulation is divided into 170×50 elements. A sensitivity analysis was conducted by doubling the number of elements in the mesh for the 5 M feed concentration case. The deviation of the results on average is less than 2.0%. The solutions are considered to be convergent when the relative error between two consecutive iterations in each field was less then 10^{-5}.

3. Results

The current model is validated by comparing the numerical results with the experimental data. Fig. 2 shows verification of the numerical results against experimental data for the polarization curve and the transient cell voltage under a constant current density operation mode. This is different from what has been done by Rice and Faghri [26] in that, in plotting the polarization curve, the cell voltage is calculated following a step that takes the current density from zero to the limiting current conditions when cell voltage comes below 0.1 V, which is consistent with the experimental method by Guo and Faghri [1]. Running under a certain current density in each time step lasts for 1 min. As illustrated in Fig. 2a, the agreement between the numerical and the experimental data is good except at low current densities, which may be caused by the Tafel kinetic assumption. In the plotting of the evolution of cell voltage, the cell voltage varies under constant current density until it falls below 0.1 V. As illustrated in Fig. 2b, the numerical results are in accordance with the experimental measurements, except for some deviations at the beginning and end stages. The deviation is mainly due to the constant reaction area assumption in the model while the effective reaction area in the catalysts varies in the experiment.

Fig. 3 displays the evolution of the cell's voltage using 1.0, 3.0, 5.0 M methanol solutions, under a constant current density of 40 mA/cm^2. The ambient temperature is assumed to be 20°C and the relative humidity is 80%. In the 5 M methanol concentration case, the cell voltage decreases during the first several minutes and then increases to a certain value after about 1 h, followed by a very slow decreasing in the next e8 h. The cell voltage decreases rapidly in the last 2 h because of the depletion of methanol in the solution. In the 3 M methanol concentration case, the cell voltage shows a similar trend as that in the 5 M methanol concentration case, it decreases during the first several minutes followed by a increase in about 1 h, then it begins a very slow decrease for about 6 h, then cell voltage decreases sharply to the limit. In the 1 M methanol concentration case, the evolution of the cell voltage exhibits a similar trend to that in 3 M and 5 M cases, while the decreasing rate of the cell voltage is much higher than the 5 M and 3 M cases and the last time is about 6.3 h. This result reveals that the fuel cell can last longer and the operational cell voltage will be more stable with a higher methanol feed concentration.

Fuel cells with higher temperatures can improve the electrochemical kinetics both in the anode and cathode, thus improving the performance of the fuel cell. On the other hand, the methanol crossover through the membrane will also increase with higher fuel cell temperatures, thus

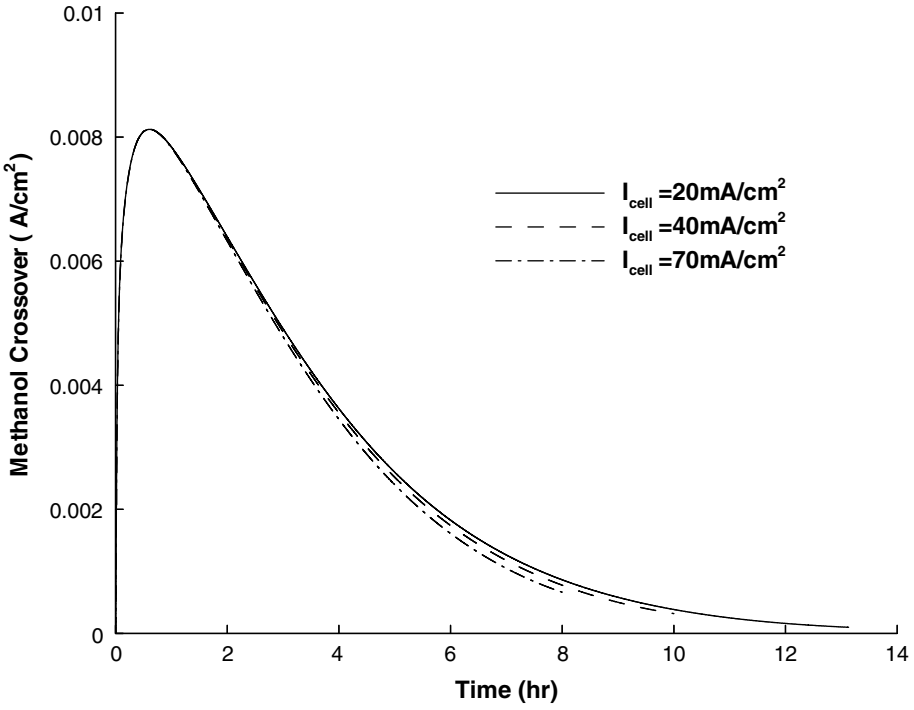

Fig. 10. Variation of total methanol crossover through membrane with different current densities and an initial feed methanol concentration of 5 M in the reservoir.

lowering the energy conversion efficiency of the fuel cell. Fig. 4 shows the temperature at the anode inlet under the same conditions as in Fig. 3. As a whole, the temperature of the fuel cell increases rapidly during the first hour and then the decreases rapidly afterward. The maximum temperature of the fuel cell increases with the increase of methanol concentration.

Fig. 5 shows the effects of methanol feed concentration on methanol crossover under the same operational conditions as in Fig. 3. The maximum crossover increases from 2 to 8 mA/cm^2 due to the significant rise of the methanol feed concentration in the reservoir. The average varying rate of methanol crossover is the lowest and the change is the smoothest in the 1 M methanol concentration case. In respect to methanol crossover, the cell performance is the best in the low feed concentration, although sustaining the output power density is the worst, as described in Fig. 3. This is the reason why the diluted methanol solution is preferred in case of a lower power DMFC.

Initially, the reservoir above the anode inlet is filled with a 10 g solution of predetermined methanol concentration. During the operation of the fuel cell, the feed concentration and the solution leftover in the reservoir decreases, because of the reaction and evaporation/condensation of methanol and water during the running process. Fig. 6 shows the evolution of feed methanol concentration and solution

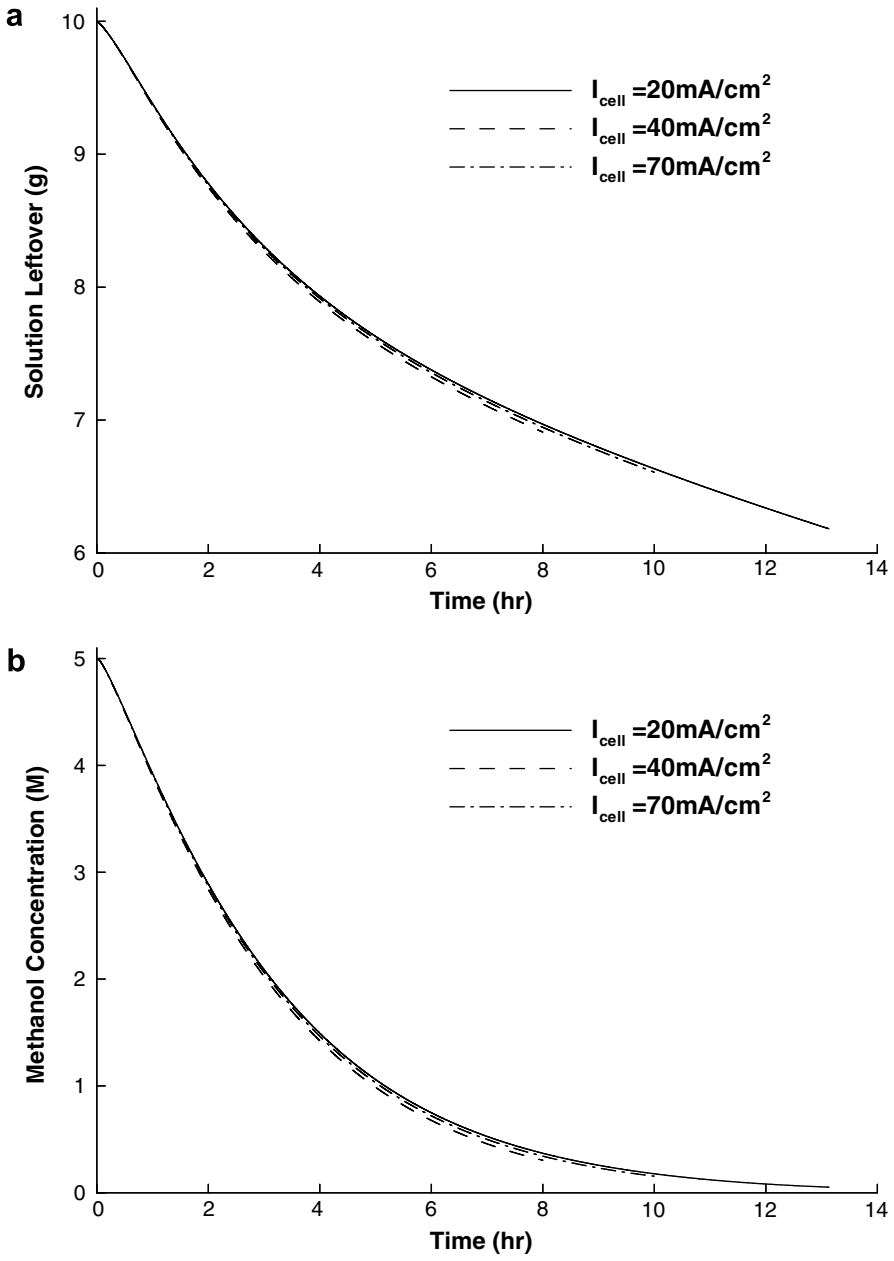

Fig. 11. Variations of (a) solution leftover; (b) methanol concentration in the reservoir with different current densities and an initial feed methanol concentration of 5 M in the reservoir.

leftover in the reservoir under the same operating conditions in Fig. 3. A higher methanol concentration results in a higher methanol permeation from the anode side to the cathode side. Therefore, the decreasing rates of the methanol concentration and the weight of the solution, increases when the initial methanol concentration in the reservoir increases. The trend of weight loss and methanol concentration variation also demonstrates that the reaction degree in the fuel cell upgrades with the increase of the feed concentration.

Eqs. (28) or (29), known as the Butler–Volmer equations, describe the electrochemical kinetics in the fuel cell. The equations basically state that the current produced by an electrochemical reaction increases exponentially with activation overpotential. Since overpotential represents voltage that is sacrificed to overcome the activation barrier associated with the electrochemical reaction, it is necessary to illustrate the reaction characteristic by overpotentials at the electrodes. Fig. 7 shows the evolution of anodic and cathodic overpotentials in the catalysts under the same operation conditions in Fig. 3. During the first several minutes, the anodic overpotential decreases rapidly, the decreasing rate increases when feed concentration increases. After first several-minute decreasing, the anodic

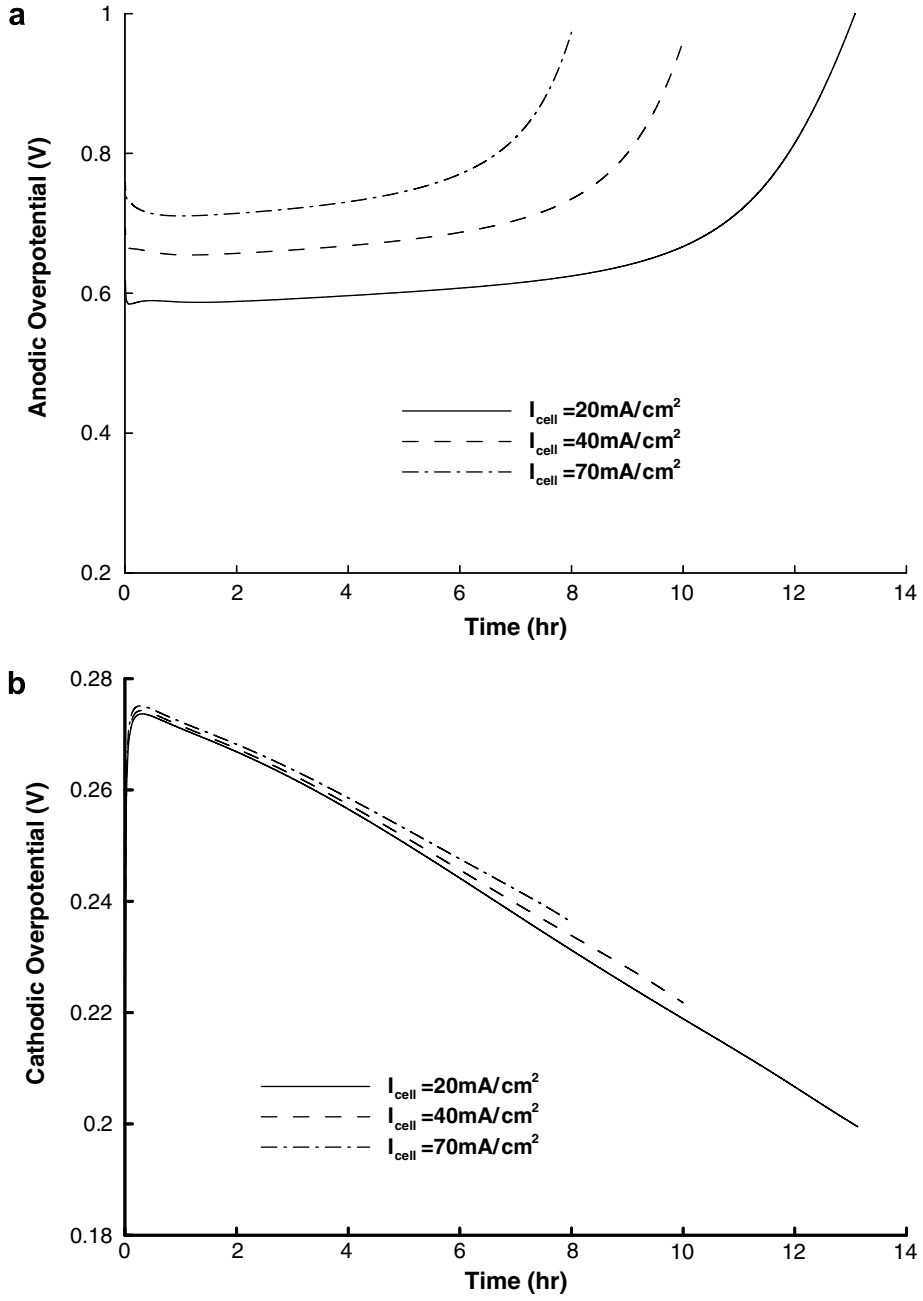

Fig. 12. Variations of (a) anodic overpotential; (b) cathodic overpotential with different current densities and an initial feed methanol concentration of 5 M in the reservoir.

overpotential increases slowly, however, the increasing rate is highest with the lowest feed methanol concentration. In the last 2 h, the increasing rate of overpotential becomes much faster, and the increasing rate becomes higher with higher feed methanol concentration. For the evolution of cathodic overpotential, during the first several minutes, the overpotential increases for the first several minutes, and then the overpotentials begin to decrease at almost the same rate. The maximum cathodic overpotential is the largest when the methanol concentration is the largest.

Fig. 8 shows the evolution of cell voltage using 5.0 M methanol solutions, under constant current densities of 20, 40 and 70 mA/cm^2. As seen from the figure, a higher current density corresponds to a lower average cell voltage. In case of 70 mA/cm^2 current density, the cell voltage decreases at the beginning and then increases slowly, followed by a sharp decrease. In case of 40 mA/cm^2 current density, the cell voltage decreases for several minutes and then increases at a decreasing rate until the curve becomes flat for almost 1 h. Afterwards, the cell voltage begins to decrease at an increasing rate, which is also followed by a rapid decrease. For all the decreasing stages that happen in the whole operation, the decreasing rate with the highest current density is the highest, thus, the operation time is the shortest. Fig. 9 shows temperature at the anode inlet under the same operating conditions in Fig. 8. The temperature increases faster for about 1 h and then decreases afterward. The temperature increases faster when the current density increases. The evolution of methanol crossover, the feed methanol concentration and solution leftover in the reservoir under different current densities is illustrated respectively in Figs. 10 and 11, under the same operating conditions in Fig. 8. The decreasing rates of methanol crossover, solution leftover and feed methanol concentration in the reservoir increase when current density increases as shown in the figures.

Fig. 12 shows the evolution of anodic and cathodic overpotentials in the catalysts under the same operating conditions in Fig. 8. The anodic overpotential decreases at the beginning and then increases at a slow rate which is followed by a rapid increase in the last 2 h. The variation rate of the anodic overpotential is the highest with the lowest current density during the running process. For the overpotential at the cathode, it initially increases at a high rate for several minutes and then decreases afterward. The increasing rate with high current density is the highest during the increasing stages of the evolution, but the decreasing rate increases when the current density decreases.

4. Conclusions

A two-dimensional, two-phase, multiple-component model has been developed for a liquid-feed DMFC system including a fuel cell and its delivery accessories. The varying methanol feed concentration in the reservoir at the anode inlet is taken into account, and the thermal effect is also considered in this model. It shows that the increasing rate of cell voltage, the temperature rise and the decreasing rate of the mass weight and methanol concentration in the reservoir are higher with a higher feed methanol concentration. The anodic overpotential increases faster with a lower feed methanol concentration, while the trend in the cathode reverses. When the value of constant current density increases, the operating time is shortened and the cell voltage decreases more quickly. The increasing rate of the temperature of the fuel cell is higher with a higher current density. The result also shows that methanol crossover increases with higher current density. It additionally shows that the methanol concentration and solution leftover in the reservoir decreases more quickly with higher current density. Similar to what happens under different feed methanol concentrations, the anodic overpotential increases faster with a lower current density, while the trend in the cathode reverses.

Acknowledgement

This research was funded by an agreement with US Army Communications-Electronics Command (CECOM) under Agreement No. DAAB07-03-3-k-415.

References

[1] Z. Guo, A. Faghri, Minature DMFCs with passive thermal-fluids management system, J. Power Sources 160 (2006) 1142–1155.
[2] Z. Guo, A. Faghri, Development of planar air breathing direct methanol fuel cell stacks, J. Power Sources 160 (2006) 1183–1194.
[3] Z. Guo, A. Faghri, Vapor feed direct methanol fuel cells with passive thermal-fluids management system, J. Power Sources 167 (2007) 378–390.
[4] Z. Guo, A. Faghri, Plannar fuel cell stack and method of fabrication of the same, Pending United States Patent 20060286436, 2006.
[5] Z. Guo, A. Faghri, Thermal-fluids management system for direct methanol fuel cells, Pending United States Patent 20060292412, 2005.
[6] Z. Guo, A. Faghri, Vapor feed fuel cells with a passive thermal-fluids management system, Pending United States Patent, 2005.
[7] G. Jewett, A. Faghri, B. Xiao, Optimization of water and air management systems for a passive direct methanol fuel cell, in preparation.
[8] X. Ren, W. Henderson, S. Gottesfeld, Electro-osmotic drag of water in ionomeric membranes, J. Electrochem. Soc. 144 (9) (1997) L267–L270.
[9] D. Chu, S. Gilman, The influence of methanol on O_2 electroreduction at a rotating Pt disk electrode in acid electrolyte, J. Electrochem. Soc. 141 (7) (1994) 1770–1773.
[10] R. Liu, P.S. Fedkiw, Partial oxidation of methanol on a metallized nafion polymer electrolyte membrane, J. Electrochem. Soc. 139 (12) (1992) 3514–3523.
[11] M.K. Ravikumar, A.K. Shukla, Effect of methanol crossover in a liquid-feed polymer-electrolyte direct methanol fuel cell, J. Electrochem. Soc. 143 (8) (1996) 2601–2606.
[12] W.F. Lin, J.T. Wang, R.F. Savinell, On-line FTIR spectroscopic investigations of methanol oxidation in a direct methanol fuel cell, J. Electrochem. Soc. 144 (6) (1997) 1917–1922.
[13] S.C. Thomas, X. Ren, S. Gottesfeld, Influence of ionomer content in catalyst layers on direct methanol fuel cell performance, J. Electrochem. Soc. 146 (12) (1999) 4354–4359.

[14] X. Ren, T.E. Springer, S. Gottesfeld, Water and methanol uptakes in nafion membranes and membrane effects on direct methanol cell performance, J. Electrochem. Soc. 147 (1) (2000) 92–98.
[15] S. Arico, P. Creti, E. Modica, G. Monforte, V. Baglio, V. Antonucci, Investigation of direct methanol fuel cells based on unsupported Pt–Ru anode catalysts with different chemical properties, Electrochim. Acta 45 (25-26) (2000) 4319–4328.
[16] M.K. Ravikumar, A.K. Shukla, Effect of methanol crossover in a liquid-feed polymer-electrolyte direct methanol fuel cell, J. Electrochem. Soc. 143 (8) (1996) 2601–2606.
[17] S.F. Baxter, V.S. Battaglia, R.E. White, Methanol fuel cell model: anode, J. Electrochem. Soc. 146 (2) (1999) 437–447.
[18] B.L. Garcia, V.A. Sethuran, J.W. Weidner, R.E. White, R. Dougal, Mathematical model of direct methanol fuel cell, J. Fuel Cell Sci. Technol. 1 (2004) 43–48.
[19] H. Dohle, J. Divisek, R. Jung, Process engineering of the direct methanol fuel cell, J. Power Sources 86 (1–2) (2000) 469–477.
[20] R. Chen, T.S. Zhao, Mathematical Modeling of a passive-feed DMFC with heat transfer effect, J. Power Sources 152 (2005) 122–130.
[21] P. Argyropoulos, K. Scott, W.M. Taama, One-dimensional thermal model for direct methanol fuel cell stacks: Part II. Model based parametric analysis and predicted temperature profiles, J. Power Sources 79 (2) (1999) 184–198.
[22] A.A. Kulikovsky, Two-dimensional numerical modeling of a direct methanol fuel cell, J. Appl. Electrochem. 30 (2000) 1005–1014.
[23] A.A. Kulikovsky, J. Dvisek, A.A. Kornyshev, Two-dimensional simulation of direct methanol fuel, cell: a new (embedded) type of current collector, J. Electrochem. Soc. 147 (3) (2000) 952–959.
[24] Z.H. Wang, C.Y. Wang, Mathematical modeling of liquid-feed direct methanol fuel cells, J. Electrochem. Soc. 150 (4) (2003) A508–A519.
[25] J. Rice, A. Faghri, A transient, multi-phase and multi-component model of a new passive DMFC, Int. J. Heat Mass Transfer 49 (25–26) (2006) 4804–4820.
[26] J. Rice, A. Faghri, Thermal and start-up characteristics of a miniature passive liquid feed DMFC system, including continuous/discontinuous phase limitations, ASME J. Heat Transfer, in press.
[27] J. Ge, H. Liu, A three-dimensional two-phase flow model for a liquid-fed direct methanol fuel cell, J. Power Sources 163 (2007) 907–915.
[28] W. Liu, C.Y. Wang, Three-dimensional simulation of liquid feed direct methanol fuel cells, J. Electrochem. Soc. 154 (3) (2007) B352–B361.
[29] C.Y. Wang, Fundamental models for fuel cell engineering, Chem. Rev. 104 (2004) 4727–4765.
[30] A. Faghri, Z. Guo, Challenges and opportunities of thermal management issues related to fuel cell technology and modeling, Int. J. Heat Mass Transfer 48 (19–20) (2005) 3891–3920.
[31] X. Ren, T.E. Springer, A. Zawodzinski, S. Gottesfeld, Methanol transport through nafionn membranes, electro-osmotic drag effects on potential step measurements, J. Electrochem. Soc. 147 (2) (2000) 466–474.
[32] A. Faghri, Y. Zhang, Transport Phenomena in Multiphase Systems, Elsevier Inc., 2006.
[33] M. Kaviany, Principles of Heat Transfer in Porous Media, second ed., Springer-Verlag, New York, 1995.
[34] A.A. Kulikovsky, J. Dvisek, A.A. Kornyshev, Modeling the cathode compartment of polymer electrolyte fuel cells: dead and active reaction zones, J. Electrochem. Soc. 146 (11) (1999) 3981–3991.
[35] J.P. Meyers, J. Newman, Simulation of the direct methanol fuel cell, Parts I–III, J. Electrochem. Soc. 149 (6) (2002) A718–A728.
[36] P. Argyropoulos, K. Scott, K. Sundmacher, A model for the liquid feed direct methanol fuel cell, J. Electroanal. Chem. 477 (2) (1999) 97–110.
[37] J. Rice, Multi-Phase, Multi-component modeling of micro-pores and porous structures, Ph.D. Thesis, University of Connecticut, 2006.